IN-SITU MELT POOL MONITORING TO OPTIMIZE LASER POWDER BED FUSION OF SCALMALLOY®

A.P. Nagalingam*, O. Poyraz*, J. Warren*, M. Shamir*, E. Yasa*, and J. Hughes*

*AMRC North-West, Roy Chadwick Way, Samlesbury Aerospace Enterprise Zone, Mellor Brook, Blackburn
BB2 7HP, United Kingdom

Abstract

In-situ monitoring techniques are gaining importance for metallic additive manufacturing methods to reduce the time spent in subsequent quality control stages. By using the data obtained from various sensing techniques, adaptive variation of process parameters can almost instantaneously be enabled with closed-loop control or machine learning algorithms can be trained. Although different systems based on thermal imaging or emissions detection have been developed mainly for process monitoring purposes, there is a need to better understand the relationship between the monitoring data and the final part quality as well as the process signatures. Thus, this study focuses on correlating the melt pool monitoring (MPM) data to material attributes to optimize laser-based powder bed fusion (PBF-LB) process parameters for a high strength Al alloy, specifically developed for PBF-LB, namely Scalmalloy®. A systematic approach modifying the laser power, hatch distance, exposure time, and scan speed was used for process parameter optimization to maximize the density. The outcomes of the MPM were compared to the post-build measurements of optical density and surface texture analysis. The findings highlight the efficacy of melt pool monitoring in guiding process optimization efforts for PBF-LB.

Keywords: Melt pool monitoring, Laser powder bed fusion, Scalmalloy, Surface roughness.

1. Introduction

The adoption of Laser based-Powder Bed Fusion (PBF-LB) additive manufacturing (AM) technique has accelerated the production of intricate components across various industries, offering design freedom and manufacturing flexibility. Among the materials explored for PBF-LB, Scalmalloy®, which is an aluminum alloy with magnesium and scandium, emerges as a promising candidate due to its exceptional mechanical properties, including high strength-to-weight ratio and corrosion resistance [1]. However, the realization of consistent manufacturing quality and mechanical performance in PBF necessitates a thorough understanding of the intricate interplay between various process parameters, defect generation mechanisms, microstructural evolution, and resultant material properties. Gas entrapment, keyhole instability, energy input and powder bed characteristics can greatly contribute to porosity and surface irregularities, affecting mechanical properties and final part quality [2]. Therefore, controlling key process parameters such as laser power, scan speed, and point distance is critical for minimizing porosity and achieving desired part properties.

Melt pool monitoring techniques play a significant role in PBF processes by enabling real-time process control, defect detection, and optimization of fabrication parameters. Thermal imaging stands out as a widely utilized method due to its non-contact nature and high spatial and temporal resolution capabilities, allowing for the precise capture of temperature distributions during the formation and solidification of melt pools [3]. By means of process monitoring and sensor data fusion, anomalies such as melt track defects were identified with 92% accuracy [4]. Studies have shown good correlation between MPM and X-ray computed tomography (XCT) results regarding porosity detection for part quality evaluation [5]. Moreover, under- and over-melting, material spatter, and delamination defects were also identified during PBF-LB [6]. Thermal imaging may encounter limitations such as sensitivity to surface conditions and limited penetration depth, potentially impacting measurement accuracy, especially in highly reflective materials or intricate geometries. Complementing thermal imaging, photodiodes, and photomultiplier tubes (PMTs) offer real-time monitoring of optical emissions generated during laser-material interaction in PBF-LB. With the help of MPM and machine learning algorithms, a true positive defect detection rate > 90 % was achieved for common defects in PBF-LB such as balling, spatter,

and micro cracks [7]. These effects were intentionally introduced by varying the laser focus leading to the changes in the melt pool shape, size, spatter, and temperature distribution-based defects.

Additionally, acoustic emission (AE) monitoring has emerged as a promising technique for melt pool characterization and defect detection in PBF-LB processes. In a study, a sampling frequency of 20 kHz recorded the characteristic amplitude data points during single layer melting of Ti6Al4V ELI material. The signals proved effective in detecting the balling phenomenon leading to the conclusion that AE-based monitoring serves as a great tool for aiding in-situ and real-time monitoring [8]. Challenges such as signal interpretation and noise reduction must be addressed to enhance the reliability and accuracy of AE-based monitoring systems. [9]. Future research directions in melt pool monitoring for PBF-LB encompass the development of multi-sensor approaches, advanced data analytics, and machine learning algorithms to further enhance real-time process control and defect prediction. Moreover, advancements in sensor technology, including high-speed cameras, fiber-optic sensors, and hyperspectral imaging, hold promise for expanding the capabilities of melt pool monitoring in PBF-LB and improving the overall quality, reliability, and efficiency of additive manufacturing processes [10]. Therefore, further research is required to understand the correlation between melt pool and mechanical properties.

In this study, a photodiode-based melt pool monitoring which is a commercially available add-on on a PBF-LB system was used to observe the impact of variations in the key process parameters for PBF-LB process development of Scalmalloy®. By monitoring melt pool characteristics such as temperature distribution, geometry, and energy deposition dynamics in real-time, optimal processing conditions with less defects were easily identified. These optimal conditions were determined based on correlations between the melt pool behavior observed and the resulting material properties experimentally evaluated through density measurements, and surface texture analysis. The integration of melt pool monitoring with traditional characterization techniques provided valuable insights on the influence of process variations on part quality, facilitating a quick route for the establishment of robust manufacturing parameters for PBF-LB of a new material.

2. Experimental Methodology

2.1. Laser-Based Powder Bed Fusion Manufacturing

Scalmalloy® powder with a particle size distribution of 20-63 μm was used on a Renishaw AM500Q Flex system to manufacture 10x10x10 mm cuboid test specimens. The PBF-LB system was programmed to maintain a consistent base plate temperature of 170°C throughout the build process while the layer thickness was kept constant at 30 μm for all experiments. A systematic approach was adopted with 12 different sets of process parameters as shown in Table 1.

Table 1. Process parameters used for manufacturing test specimens.

S. No	Laser power (W)	Hatch distance (mm)	Exposure time (μs)	Point distance (mm)	Scan speed (mm/s)	Energy density (J/mm^3)	Difference compared to baseline
1	320	0.09	40	0.08	1429	83	(+10 %) scan speed
2	320	0.09	46	0.08	1290	92	**Used as a baseline**
3	320	0.09	52	0.08	1176	101	(-10 %) scan speed
4	350	0.09	46	0.08	1290	101	(+10 %) Laser power
5	290	0.09	46	0.08	1290	83	(-10 %) Laser power
6	320	0.1	46	0.08	1290	83	(+10 %) Hatch distance
7	320	0.08	46	0.08	1290	103	(-10 %) Hatch distance
8	350	0.09	40	0.08	1429	91	(+10 %) scan speed and laser power
9	320	0.08	40	0.08	1429	93	(+10 %) scan speed and (-10%) hatch distance
10	380	0.145	39	0.08	1455	60	(~ +20 % laser power, + 60 % hatch distance)
11	320	0.09	63	0.08	1013	117	(~ +40% exposure time)
12	320	0.09	52	0.1	1389	85	(+25 % point distance)

The build direction (Z-axis) was set parallel to the normal of one of the cube planes and without any angular orientation in the XY plane as shown in Figure 1. Throughout the fabrication process, gas flow was maintained at a constant rate of 190 m^3/h to provide a stable processing environment. The specimens were then removed from the base plate using wire-electric discharge machining.
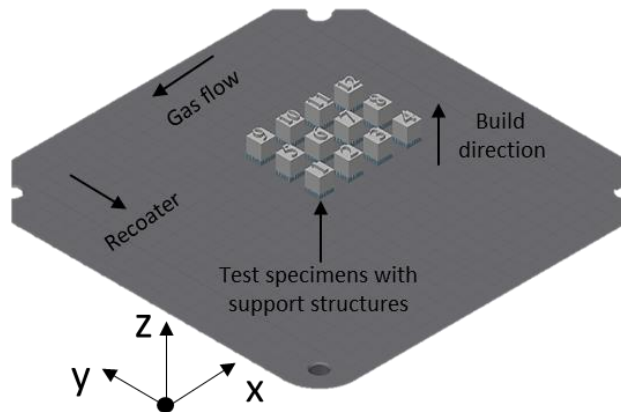

Figure 1. Test specimen arrangement on the base plate.

2.2. Melt Pool Monitoring and Analysis Methodology

Figure 2. shows the schematic outline of the spectral melt pool monitoring system composed of three photodiode sensors for detecting the radiation from the melt pool with different wavelengths, such as near-visible (700-1050 nm) and infrared regions (1080-1700 nm). The sampling rate of the sensors was set to 100 kHz. The recorded readings with respect to time were processed and mapped in XYZ coordinates.
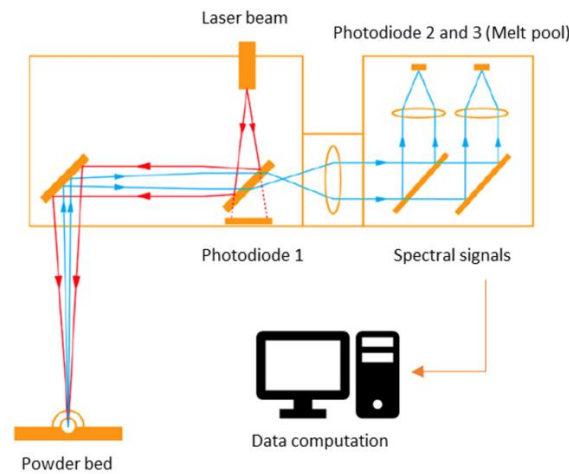
Figure 2. Schematic outline of the spectral melt pool monitoring system in powder bed fusion.

As shown in Figure 3, the readings in a monitoring area are investigated in pixels with a size of 150x150 μm or 40x40 μm depending on the value to be calculated. Within each pixel, the sum value of all recorded data (MP-Sum) is calculated taking a pixel size of 40x40 μm size whereas the maximum value (MP-Max) is calculated within a single pixel with a size of 150x150 μm. Renishaw's InfiniAM Meltpool view software allows analysis of the MP-Sum and MP-Max values with respect to XYZ coordinates, which can be referred to as data mapping.

2.3. Characterization Methodology

The side surfaces of the specimens were subjected to surface texture analysis per ISO 257178-2 and ISO 25178-3. The measurement area on each side surface was fixed as 3.5×2.5 mm for surface quality assessment. The most widely used areal surface textures such as *Sa* (arithmetic mean deviation of the surface) and *Sz* (arithmetic mean height of the surface) were extracted to understand the effect of process parameters on the resulting surface quality.
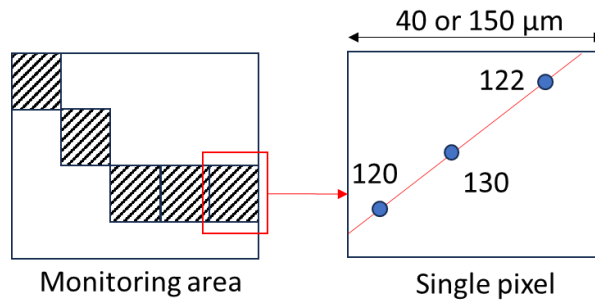

Figure 3. Data monitoring and computation methodology in melt pool monitoring system

The specimens were then finish machined on a Hermle C400 with a Ø8 mm end-mill at 8000 rpm spindle speed and 50 mm/min table feed to improve the surface quality and to remove any sintered powder or foreign material so to have reliable density measurements. Density measurements using Archimedes' principle were then conducted per ASTM 962-23 on a precision balance (Precisa Series 360 EP 125 SM) in distilled water. Finally, the specimens were cross sectioned at 5 mm from top surface, polished and the porosity was calculated based on the cross-sectional images as shown in Figure 4.
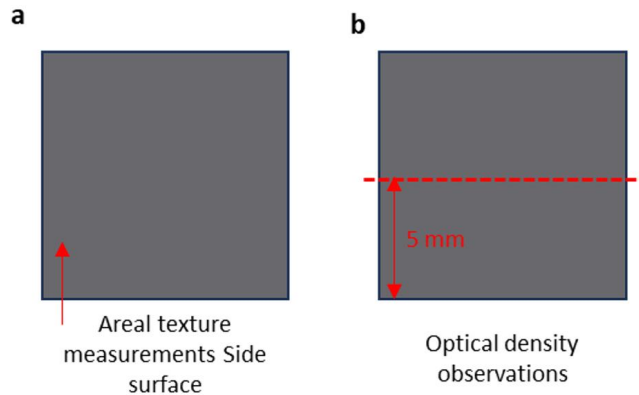

Figure 4. (a) Areal texture measurement at side surface; (b) Optical density measurement plane

The MPM data from the PBF-LB process was then extracted and processed to identify any anomalies caused by the processing conditions. These were then compared against the density and optical surface micrographs to identify any relations in terms of process anomalies. The results were then compared and analyzed to down select the best parameters for further processing using Keyence VHX-7000 software.

3. Results and Discussions

3.1. Anomaly Detection Using Melt Pool Monitoring

Figure 5 presents the melt pool analysis in the InfiniAM Meltpool view, derived from spectral signatures recorded using photodiodes in the infrared wavelength range of 1080-1700 nm. A small pixel size of 40x40 μm, along with the spectral MP-Sum value, was used, ensuring optimal pixel size as described in Figure 3. The spectral emissions distinctly differentiate between specimens, reflecting variations in processing conditions such as laser power, hatch distance, exposure time, and thus scan speed.
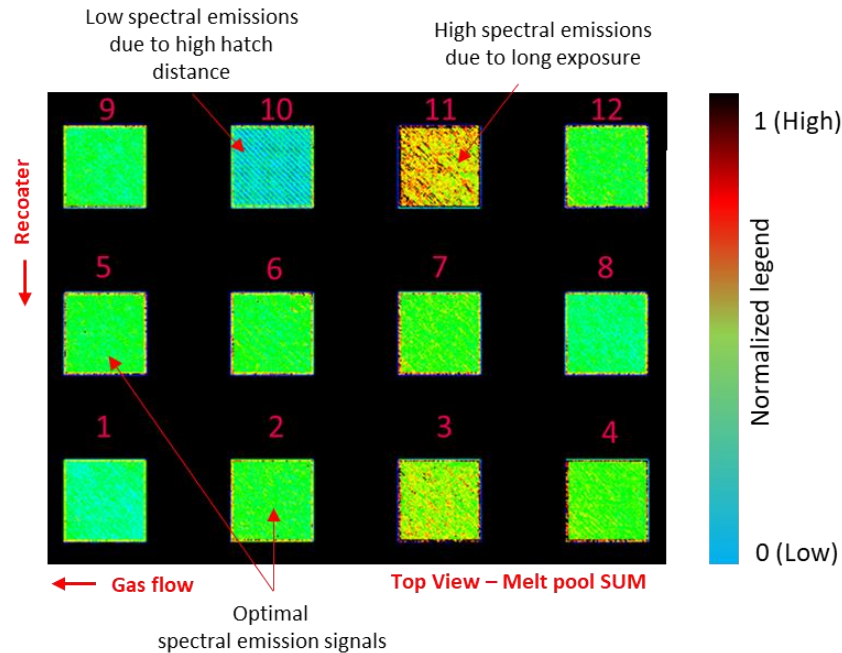
Figure 5. Melt pool spectral intensity difference between each test specimen with varying process parameters.

Figure 6 illustrates the top (XY) and front (XZ) views of specimens with varying process parameters namely the scan speed and laser power. A laser power of 320 W serves as the baseline, as established in existing literature [11]. A comparative analysis of specimens #5 (290 W), #2 (320 W), and #4 (350 W) revealed intriguing insights. It was noted that the spectral emission intensity of specimen #4 surpassed that of #2 and #5, indicating high heat input and the potential possibility for thermal defects such as keyhole porosity in the specimen. However, emission intensity for a laser power range 290 to 320 W at a constant scan speed of 1290 mm/s did not indicate any significant change in the MPM data. This also leads to a conclusion that a 10 % change in the laser power, may not be captured by the MPM data if it is aimed to be used a s a stringent process control tool. Experiments involving a variation of laser power at another fixed scan speed of 1429 mm/s, as shown in Figure 6a with specimens #1 and #8, demonstrated lower spectral emissions compared to the baseline specimen #2. This discrepancy suggests reduced temperature distributions attributable to the higher scan speed as expected. Again, there is no significant change in the obtained MPM data between specimens #1 and #8 which are differentiated by a 10 % change in the laser power.

Subsequently, the scan speed was varied within the range of 1013-1429 mm/s while maintaining a fixed laser power of 320 W as shown in Figure 6. Analysis of specimens #3 (1170 mm/s), #2 (1300 mm/s), and #1 (1430 mm/s) revealed a consistent trend: as scan speed increased, melt pool spectral emission intensity decreased. This observation underscores the inverse relationship between scan speed and heat distribution, emphasizing the

importance of achieving optimal and uniform heat distribution to mitigate keyhole and porosity defects while enhancing mechanical properties.
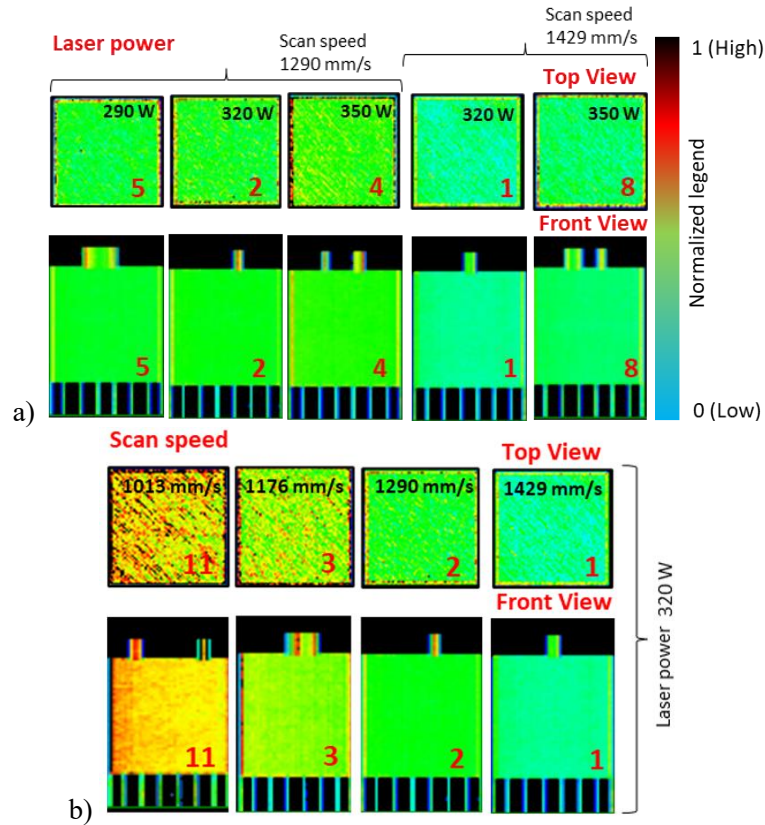

Figure 6. Melt pool spectral intensity at varying (a) Laser powers and (b) Scan speeds.

The effect of hatch distance was also investigated, ranging from 0.08 to 0.1 mm, while maintaining a fixed laser power of 320 W and scan speed of 1300 mm/s as shown in Figure 7. Comparative analysis of specimens #7, #2, and #6 revealed no significant changes in melt pool intensity or temperature distributions. This lack of variation can be attributed to the optimal laser spot size of 0.08 mm in the Renishaw 500Q Flex system, where minor alterations in hatch distance at a scan speed of 1290 mm/s did not significantly impact melt pool morphology. However, a notable discrepancy emerged when the hatch distance was increased to 0.145 mm in specimen #11. Here, low-intensity signals and substantial gaps between each hatch were observed, indicating uneven melting, and suggesting the likelihood of lack-of-fusion defects.

Additionally, the exposure time was varied within the range of 40-63 µs, while maintaining a laser power of 320 W, hatch distance of 0.09 mm, and point distance of 0.08 mm. A progressive increase in spectral intensity was observed with an increase in exposure time. As exposure time increased across specimens #1, #2, #3, and #11, melting time, heat input, and melt pool size increased accordingly. However, unstable melt pool characteristics associated with prolonged exposure times are thought to result in over-melting of certain regions, resulting in keyhole defects. Based on the melt pool spectral observations, an exposure time of 46 µs demonstrated uniform heat distribution throughout the specimen, highlighting its potential for optimizing process parameters and mitigating defects in laser powder bed fusion.
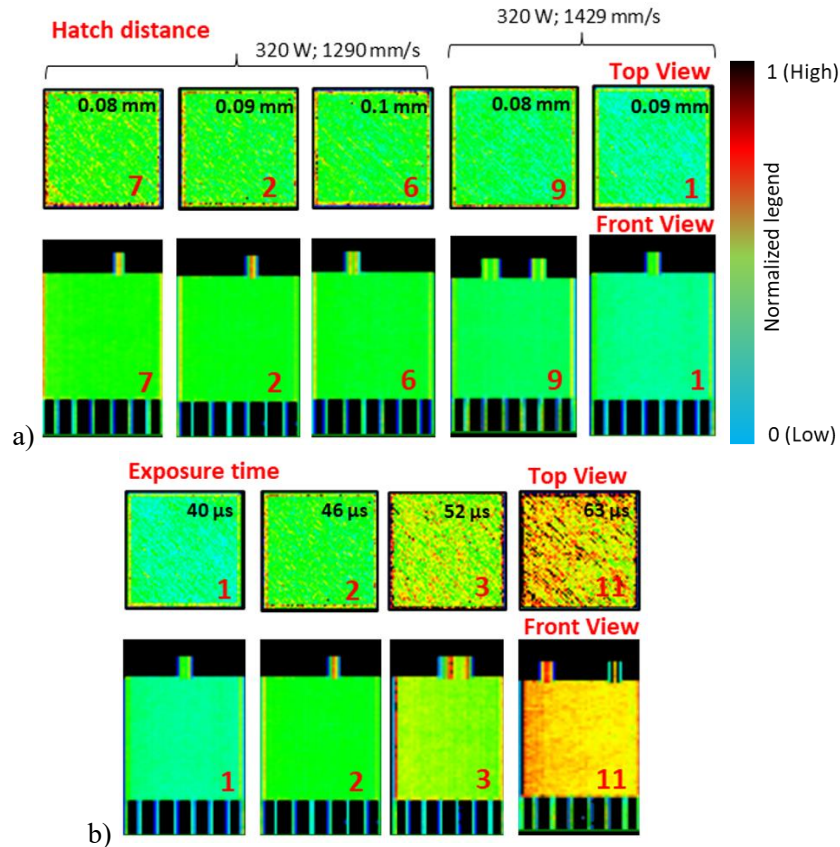
Figure 7. Melt pool spectral intensity at varied (a) hatch distance and (b)exposure time.

3.2. Surface Texture and Density Measurements

Areal surface textures, represented by parameters Sa and Sz, were measured across the four side surfaces of the specimens to understand the influence of processing conditions. As depicted in Figure 8, optical topography images of samples #2, #10, and #11, representing optimal melting conditions with uniform spectral emission, the highest hatch distance, and the highest exposure time, respectively, were analyzed.

No significant differences in topography characteristics were observed among the specimens. This consistency can be ascribed to the application of a border scan method that guaranteed uniform surface quality across the specimens by using a constant laser power of 360 W, point distance of 80 μm, and exposure period of 40 μs during scanning. The arithmetic mean deviation (Sa) and arithmetic mean height (Sz) were found to range between ∼ 30-40 μm and ∼ 230-300 μm, respectively, across the side surfaces. Notably, statistical analysis revealed no significant differences between various parameter selections. The top surfaces were not measured since numbers were embossed on them to differentiate each specimen.
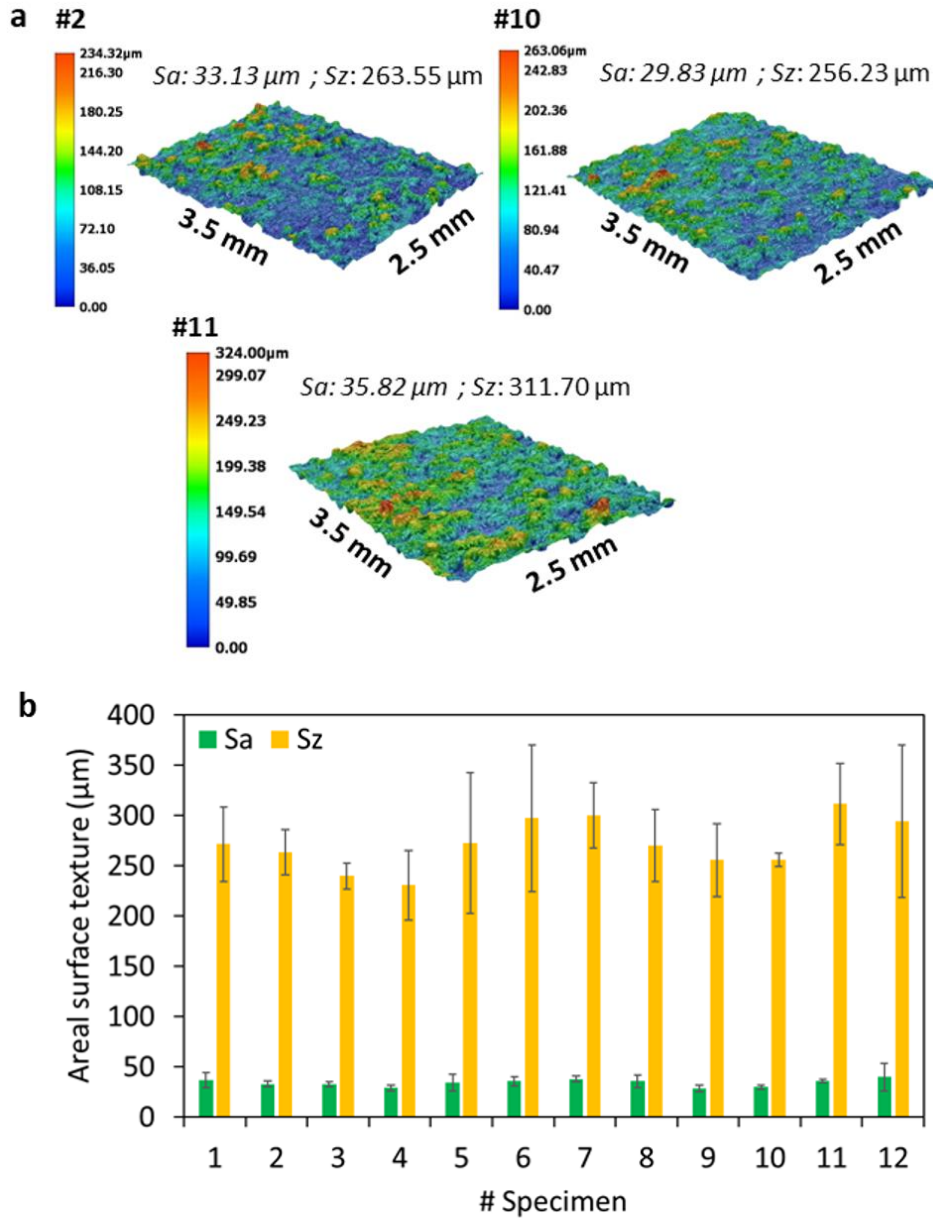
Figure 8. (a) Areal surface topography of selected parameter sets and, (b) surface textures Sa and Sz of the specimen side surfaces (error bars represent standard deviation in the measurements).

Next, Archimedes results were analyzed for evidence of process anomalies as shown in Figure 9. The measurements were conducted machined specimens so that the surface irregularities do not affect the reliability of the process. The obtained density measurements were consistent with the findings from melt pool spectral intensity.

Both the lowest and the highest part density values were obtained by applying extreme parameter sets with the lowest and highest energy density values to specimens #10 and #11, respectively. By examining the lowest and highest spectrum emissions in the MPM data, this result was also anticipated during the MPM stage. This leads to the conclusion that the extreme conditions especially with low density parts can be observed analyzing MPM data to have conclusive results without any post-build material characterizations. Using MPM data, it was also possible to expect a minor difference in part density between specimen #1 and specimen #2 due to a slight increase in scanning speed and a reduction in energy input. Specimen #2, which exhibited full green

spectral emissions, had a part density of 2.645 g/cm³, whereas specimen #1, which showed scattered low spectral emissions with a cyan color, had a density of 2.641 g/cm³. Still, some examples like specimen #4 and specimen #7 having higher laser power and smaller hatch distance to generate more energy input, showed lowest part densities than specimen #1 and specimen #2. To understand the relationship between MPM and part density results, additional microstructural investigations were conducted. The compiled data, which includes microstructural views, energy density, part density, and spectral emission benchmarks, are presented in Table 2.
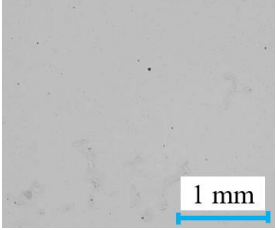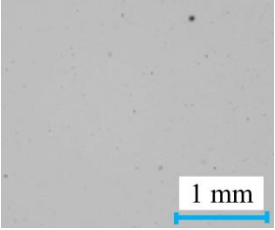

	1	2	3	4	5	6	7	8	9	10	11	12
Machined	2.641	2.645	2.644	2.623	2.647	2.641	2.638	2.635	2.640	2.618	2.646	2.641
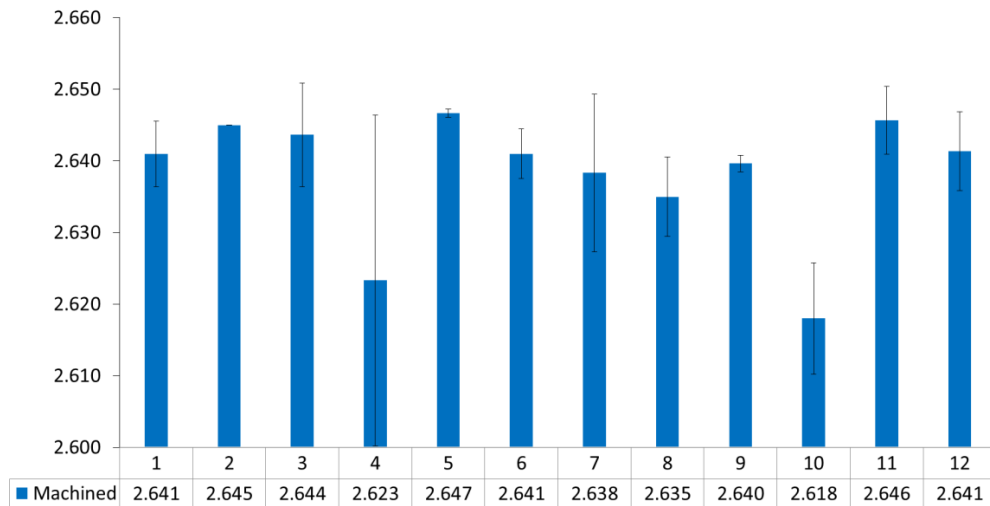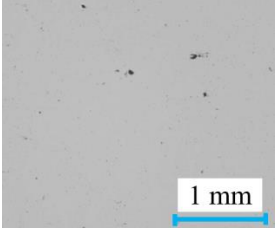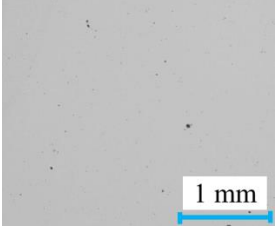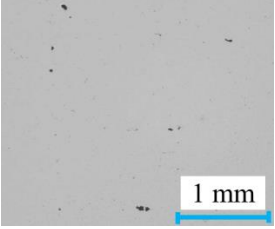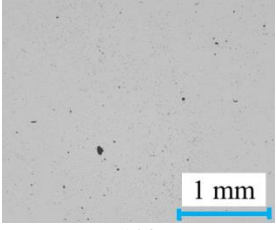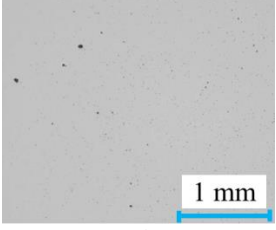
Figure 9. Density measurement results for machined specimens (error bars represent measurement error).

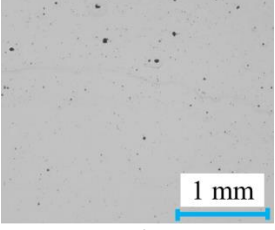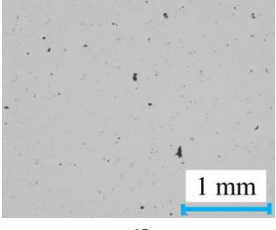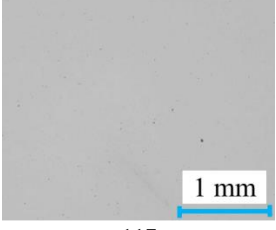With this aim, the cross-sections of the specimens were analyzed for defects such as lack-of-fusion, and keyhole porosity defects due to changes in the process parameters. Some anomalies present in the specimen surfaces are shown in Table 2. Lower energy input (83 - 85 J/mm³) with 10 % higher scanning speed resulted in reduced part density for specimen #1, and for specimen #12 with a scanning speed increased by almost 8 % due to change of point distance. Similar to these two cases, specimen #6 also showed a loss in density when the hatch distance was raised by 10%, resulting in an energy input of only 83 J/mm³. The analysis of the optical microscopy images of specimens #1 and #6 given in Table 2 reveals large and irregular porosities, i.e. lack of fusion. The MPM data also showed lower or low-moderate spectral emissions for those specimens well aligned with the experimental observations.

However, specimen #5, with a 10% decrease in laser power, leading to an energy density of 83 J/mm³, showed optimal spectral emissions and no decrease in part density. This is a clear indication that the volumetric energy density cannot solely be used for process parameter optimization. Moreover, how the energy density is changed, e.g. by changing the laser power or point distance or exposure time, makes a difference in terms of porosity formation as also addressed in a relevant study [12].

Conversely, the application of increased energy input through parameter modification have not produced the best part density outcomes. An excellent illustration of how to increase the energy input levels to 103 J/mm³ while maintaining a density of only 2.638 g/cm³ is specimen #7, which has a reduced hatch distance of 0.08 mm. For specimens #4 and #8 (10 % increase in both scan speed and laser power), further density issues were also noted while using a higher laser power of 350 W. The optical microscopy images of specimens #4 and #7, which were exposed to high laser power or energy input, showed scattered and spherical pores, indicating gas entrapment and process instabilities. Regarding the MPM data, specimen #4 and #7 both exhibited moderate to high levels of spectral emissions. The core regions of these specimens were represented in green color with intermittent yellow spots, whereas the outer surfaces demonstrated gradients between yellow to red. Specimen #8 was a unique case. Despite having a higher laser power, the increase of the scanning speed caused lack of fusion voids, as evidenced by the low to moderate emissions observed during the MPM phase.

Table 2. Energy density, part density, microstructures and emission benchmarks

Specimen No.	#1	#2	#3
Microstructure			
Energy Density (J/mm^3)	83	92	101
Part Density (g/cm^3)	2.641	2.645	2.644
Emission Benchmark	Lower	Moderate	Higher
Specimen No.	**#4**	**#5**	**#6**
Microstructure			
Energy Density (J/mm^3)	101	83	83
Part Density (g/cm^3)	2.623	2.647	2.641
Emission Benchmark	Moderate-High	Moderate	Low-Moderate
Specimen No.	**#7**	**#8**	**#9**
Microstructure			
Energy Density (J/mm^3)	103	91	93
Part Density (g/cm^3)	2.638	2.635	2.64
Emission Benchmark	Moderate-High	Low-Moderate	Low-Moderate
Specimen No.	**#10**	**#11**	**#12**
Microstructure			
Energy Density (J/mm^3)	60	117	85
Part Density (g/cm^3)	2.618	2.646	2.641
Emission Benchmark	The lowest	Highest	Low-Moderate

4. Conclusions

In this study, in-situ melt pool monitoring of PBF-LB proved as a suitable tool for process parameter optimization of Scalmalloy® aluminium alloy. Key process parameters such as laser power, hatch distance, exposure time, scanning speed, and point distance were varied to optimize the manufacturing process. Significant differences were observed from the melt pool spectral intensity signals while varying the process parameters. Using traditional material characterization techniques, the observations from the melt pool spectral analysis were

confirmed to be beneficial for giving the right direction for process optimization The optical micrographs provided evidence of process anomalies such as gas pores, fusion defects, keyhole, and lack-of-fusion defects. Overall, melt pool spectral intensity analysis based on photodiodes has been found to be practical to understand the underlying physical characteristics during new material development and process optimization, effectively reducing the time required spent on traditional characterization methods.

References

1. Cabrera-Correa, L., et al., Pitting and intergranular corrosion of Scalmalloy® aluminium alloy additively manufactured by Selective Laser Melting (SLM). Corrosion Science, 2022. 201: p. 110273.

2. Muhammad, M., et al., A comparative investigation on the microstructure and mechanical properties of additively manufactured aluminum alloys. International Journal of Fatigue, 2021. 146: p. 106165.

3. McCann, R., et al., In-situ sensing, process monitoring and machine control in Laser Powder Bed Fusion: A review. Additive Manufacturing, 2021. 45: p. 102058.

4. Harbig, J., et al., Methodology to determine melt pool anomalies in powder bed fusion of metals using a laser beam by means of process monitoring and sensor data fusion. Materials, 2022. 15(3): p. 1265.

5. Reijonen, J., A. Revuelta, and H.P.N. Nagarajan, Towards data driven quality monitoring: alignment and correlation of photodiode-based co-axial melt pool monitoring signals to part quality in laser powder bed fusion. IOP Conference Series: Materials Science and Engineering, 2023. 1296(1): p. 012009.

6. Yang, L., et al., Monitoring and detection of meltpool and spatter regions in laser powder bed fusion of super alloy Inconel 625. Progress in Additive Manufacturing, 2020. 5(4): p. 367-378.

7. Gaikwad, A., et al., Multi phenomena melt pool sensor data fusion for enhanced process monitoring of laser powder bed fusion additive manufacturing. Materials & Design, 2022. 221: p. 110919.

8. Kouprianoff, D., et al., Monitoring of laser powder bed fusion by acoustic emission: Investigation of single tracks and layers. Frontiers in Mechanical Engineering, 2021. 7: p. 678076.

9. Seleznev, M., et al., In situ detection of cracks during laser powder bed fusion using acoustic emission monitoring. Additive Manufacturing Letters, 2022. 3: p. 100099.

10. McCann, R., et al., In-situ sensing, process monitoring and machine control in Laser Powder Bed Fusion: A review. Additive Manufacturing, 2021. 45: p. 102058.

11. Lasagni, F., et al., On the processability and mechanical behavior of Al–Mg–Sc alloy for PBF-LB. Progress in Additive Manufacturing, 2022. 7(1): p. 29-39.

12. Yasa, E., et al., The Laser Powder Bed Fusion Process Development of 17-4 PH Stainless Steels with Pulsed-Wave Lasers. Solid Freeform Fabrication 2021: Proceedings of the 32nd Annual International Solid Freeform Fabrication Symposium – An Additive Manufacturing Conference.